Superconducting resonator circuits at frequencies above the gap frequency

de Lange, G.; Kuipers, J. J.; Klapwijk, T. M.; Panhuyzen, R. A.; van der Stadt, H.; de Graauw, M. W. M.

Published in:
Journal of Applied Physics

DOI:
10.1063/1.358876

Publication date:
1995

Superconducting resonator circuits at frequencies above the gap frequency

G. de Lange, J. J. Kuipers, T. M. Klapwijk, R. A. Panhuyzen, H. van de Stadt, and M. W. M. de Graauw

Citation: Journal of Applied Physics **77**, 1795 (1995); doi: 10.1063/1.358876
View online: https://doi.org/10.1063/1.358876
View Table of Contents: http://aip.scitation.org/toc/jap/77/4
Published by the American Institute of Physics

Superconducting resonator circuits at frequencies above the gap frequency

G. de Lange,[a] J. J. Kuipers, and T. M. Klapwijk
Department of Applied Physics and Materials Science Center, University of Groningen, Nijenborgh 4, 9747 AG Groningen, The Netherlands

R. A. Panhuyzen, H. van de Stadt, and M. W. M. de Graauw
Space Research Organisation of the Netherlands, Landleven 12, 9747 AD Groningen, The Netherlands

(Received 11 May 1994; accepted for publication 7 November 1994)

The frequency response of three superconductive niobium resonating circuits, formed by a Nb microstrip and a Nb tunnel junction, is measured and analyzed at frequencies above the superconducting gap frequency. The circuits are placed in a waveguide system and the frequency response is determined with a Fourier transform spectrometer. The calculated and measured resonance frequencies and bandwidths are in good agreement with the extreme anomalous limit of the Mattis–Bardeen theory on the anomalous skin effect in superconductors [D.C. Mattis and J. Bardeen, Phys. Rev. **111**, 412 (1958)]. The observed loss is higher than predicted by this theory, in agreement with previous observations on Nb films. The use of other materials for striplines as tuning circuits for heterodyne superconducting tunnel junction mixers is analyzed. © *1995 American Institute of Physics.*

I. INTRODUCTION

Superconductive striplines have shown to be of major importance in the coupling of high frequency signals to Superconducting-Insulator-Superconducting (SIS) quasi-particle mixers. Quasi-particle mixers are currently the most sensitive heterodyne mixers in the 90–800 GHz frequency range. They consist of a sandwich (of area $\approx 1\,\mu m^2$) made of two superconducting layers separated by a very thin oxide layer (2 nm) and therefore have a relatively high intrinsic capacitance. For an efficient coupling of high frequency radiation, a tuning circuit has to be provided which tunes out this capacitance. For frequencies in the millimeter range (<300 GHz) this can be achieved with mechanical tuners in a waveguide system, but this tuning becomes increasingly more difficult and narrow-banded at higher frequencies. Räisänen *et al.*[1] proposed the use of on-chip superconducting striplines as tuning elements at 100 GHz and several groups now successfully employ niobium integrated tuning elements at frequencies up to 600 GHz.[2–4]

The characteristic energy-gap frequency ($f_{gap}=2\Delta/h$, $\Delta=$ the minimum energy of one quasi-particle excitation) of niobium is 680 GHz and at frequencies well below f_{gap}, niobium striplines behave as ideal loss and dispersion free striplines. At frequencies near f_{gap}, Nb striplines become lossy and dispersion occurs. Far above the gap frequency superconducting Nb behaves as a normal conductor with a relatively low conductivity and at these frequencies other materials, as gold or aluminium, seem to be favorable to be used for the tuning structures. It is therefore of interest to know how the onset of dispersion and loss degrades the Nb stripline performance and at what frequency the use of other materials becomes attractive.

The behavior of superconducting striplines was mainly investigated for use in digital and analog circuits up to 20 GHz.[5,6] Kautz[7,8] made a theoretical investigation of picosecond pulse transmission on both normal and superconducting striplines. Javadi *et al.*[9] recently measured the onset of dispersion in a 500–1000-μm-long Nb stripline by measuring the mode spacing of 50 GHz fundamental Josephson oscillation modes up to 800 GHz. Hu *et al.*[10] and Dierichs *et al.*[11] used a Fourier transform spectrometer (FTS) to investigate the harmonic behavior of Nb striplines with fundamental resonance frequencies of 100 and 345 GHz, but no resonances near f_{gap} were observed.

The measurement of the absorption at frequencies above the gap frequency brings our work in relation with the early work of Glover and Tinkham [12] and Richards and Tinkham[13] on the FIR transmission and absorption properties of superconductors. Their work revealed for the first time the dramatic changes in the electromagnetic properties in thin film superconductors near f_{gap} and was actually the first direct observation of the superconducting energy-gap. The behavior of Nb near f_{gap} was later investigated by Norman[14] with a calorimetric measurement on 250-nm-thick films and more recently by Nuss *et al.*[15] who used terahertz time domain measurements on 15-nm-thin Nb films.

In this paper we report on the FTS measurements of Nb tuning structures with resonance frequencies around the gap frequency. The frequency response of the tuning structure is measured by using the SIS-junction as a direct detector. We observe clear resonances of the tuning structures above the gap frequency and we compare our data with the microscopic theory for the electromagnetic behavior of superconducting materials, developed by Mattis and Bardeen.[16] Section II describes the general behavior of the striplines and the tuning circuits. In Sec. III the influence of the surface impedance on the performance of the tuning circuits is analyzed. A comparison between normal metal and superconducting

[a]Present address: Research Laboratory of Electronics, Massachusetts Institute of Technology, Cambridge, MA 02139.

 0021-8979/95/77(4)/1795/10/$6.00

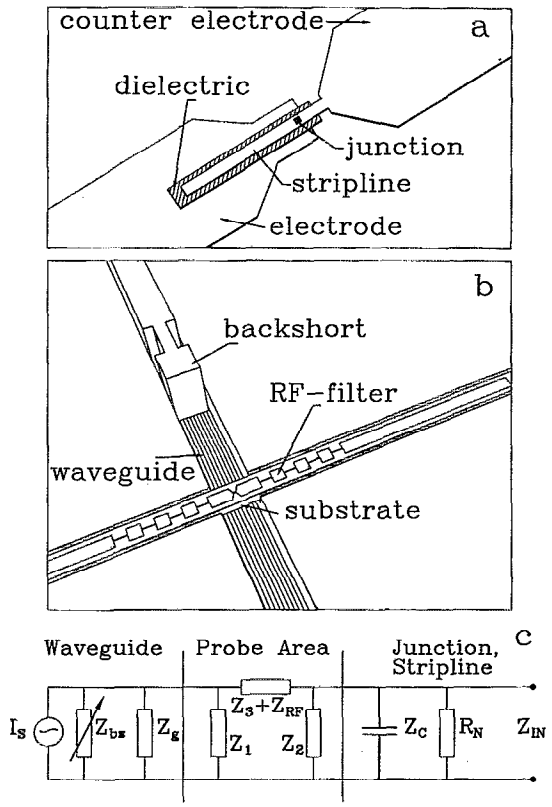

FIG. 1. (a) General geometry of the stripline resonator circuit. (b) Detail of the geometry of the mixerblock in the region close to the junction. (c) Lumped element equivalent circuit of the junction and the waveguide mount.

striplines is made in Sec. IV and Sec. IV A. gives an estimation of the performance of a heterodyne receiver which utilizes these striplines. The experimental details of the FTS measurement setup and the waveguide mixer are described in Sec. V. The results of the FTS measurements and the analysis of the data are given in Secs. VI and VII.

II. STRIPLINES

The general geometry and definition of the dimensions of the resonating circuits we report on is shown in Fig. 1(a). As can be seen in the figure, the resonating circuit is implemented by extension of the upper electrode over the counter electrode. The wave propagation in the stripline is characterized by the propagation constant

$$\gamma=\sqrt{ZY}=\alpha+j\beta \tag{1}$$

and the characteristic impedance

$$Z_0=\sqrt{\frac{Z}{Y}}, \tag{2}$$

where Z and Y are the series impedance and shunt admittance per unit length of the line.[17] The phase velocity v_p of the electromagnetic wave in the stripline is related to the wave number β (the imaginary part of γ) via $v_p=\omega/\beta$, where ω is the angular frequency. The real part of $\gamma(=\alpha)$ is the attenuation constant. The shunt admittance Y per unit length (assuming negligible fringing fields and no losses in the dielectric) is given by

$$Y=j\omega\left(\frac{W}{d}\right)\epsilon_0\epsilon_r, \tag{3}$$

where W is the width of the stripline, d is the thickness of the dielectric, ϵ_r is the relative dielectric, constant of the dielectric, and ϵ_0 is the permittivity of free space. The series impedance Z is given by

$$Z=j\omega\mu_0\left(\frac{d}{W}\right)+\frac{Z_{s1}+Z_{s2}}{W}, \tag{4}$$

where Z_{s1}, Z_{s2} are the surface impedances of the strip and the ground plane (the electrode and the counter-electrode) and μ_0 is the permeability of free space. The first term of Z covers the geometrical inductance of the line, whereas the second part is determined by the surface currents of the microstrip and therefore by the material parameters.

The input impedance Z_{IN} of a stripline with length l, terminated with a load impedance Z_L is calculated with

$$Z_{IN}=Z_0\left(\frac{Z_L\cosh(\gamma l)+Z_0\sinh(\gamma l)}{Z_0\cosh(\gamma l)+Z_L\sinh(\gamma l)}\right). \tag{5}$$

In the configuration shown in Fig. 1(a), the stripline is placed in parallel with the junction. By choosing the design parameters such that at the desired frequency the stripline has an inductive input impedance which tunes out the intrinsic capacitance of the junction, the stripline is used as a tuning circuit.

The frequency dependence of the tuning structure is analyzed by calculating the coupling of the "matched" junction impedance $Z_m(\omega)$, formed by the junction and the matching circuit, to a signal source with driving impedance $Z_{wvg}(\omega)$. The coupling efficiency $C(\omega)$ of signal power into the matched junction is given by

$$C(\omega)=1-\left|\frac{Z_{wvg}(\omega)-Z_m^*(\omega)}{Z_{wvg}(\omega)+Z_m^*(\omega)}\right|^2. \tag{6}$$

$Z_m(\omega)$ is calculated from the combination of the stripline impedance [Eq. (5)] and the junction impedance $Z_j(\omega)$, where we take for $Z_j(\omega)$ the impedance of the parallel combination of the junction normal state resistance R_N and the junction capacitance C_j (omission of the actual quantum impedance of the tunnel junction[10] has only minor effects):

$$Z_j(\omega)=\frac{R_N}{1+j\omega R_N C}. \tag{7}$$

The design parameters for the striplines are the length L and the width W. All other parameters, which will be discussed later, are set by the junction fabrication process. The frequency dependence of the equivalent source impedance $Z_s(\omega)$ of the waveguide system we use, will be described in Sec. VII.

The three different types of tuning structures reported on in this work, the "end-loaded", the "open-ended", and the 'two-section' tuning, are shown in the insets of Figs. 8, 9, and 10. The matched junction impedance $Z_m(\omega)$ of the open-

ended stub is formed by the parallel combination of $Z_j(\omega)$ and $Z_{IN}(L,W,\omega,Z_L)$, where the load impedance Z_L of the stripline is set to $10^6\ \Omega$. The length L is chosen such that the input impedance of the line is inductive, and has a value which cancels the junction capacitance C_j. In the two-section stub design, the matching to the junction is also achieved by the parallel combination of the junction with the stripline, but now the stripline consists of a wide and narrow section. The input impedance of the line is given by $Z_{IN}=Z_{IN}[L_1,W_1,\omega,Z_{IN}(L_2,W_2,\omega,\infty)]$, where L_1, W_1 and L_2, W_2 are the dimensions of the narrow and wide sections, respectively. The wide section is a quarter wavelength long (at the design frequency) and this provides a shorted load impedance for the narrow section. The length of the (inductive) narrow section is again adjusted such that the capacitance is tuned out. In the end-loaded stub design, the junction is not placed at the beginning of the stripline, but at the end. The stripline now acts as an impedance transformer, which transforms both the resistance and the reactance of the junction. The input impedance of the line is given by $Z_{IN}(\omega)=Z_{IN}[L,W,\omega,Z_j(\omega)]$.

The coupling coefficient $C(\omega)$ defined in Eq. (6) gives the coupling of signal power into the combination of the junction and the tuning circuit. This equals the actual coupling of power into the junction ($=P_{junc}$) only if the tuning circuit is lossless, a condition which is fulfilled for superconducting striplines well below the gap frequency. In striplines made of normal metals and in superconducting striplines used above the gap frequency, the losses of the matching circuit have to be taken into account. Therefore we calculate the quantity C_{rel}, which gives the relative amount of power coupled into the junction. If the total amount of coupled power in the matching circuit and the junction is P_{tot}, then C_{rel} is defined such that the actual amount of power coupled to the junction is given by $P_{junc}=P_{tot}C_{rel}$. For the parallel combination of the junction and the open-ended or the two-section stub C_{rel} is given by:

$$C_{rel}=\frac{\mathrm{Re}(Y_j)}{\mathrm{Re}(Y_j+Y_{IN})} \tag{8}$$

with $Y_j=Z_j^{-1}$ and $Y_{IN}=Z_{IN}^{-1}$. For the calculation of C_{rel} in the end-loaded stripline, an equivalent π-network of the stripline is used. The resulting C_{rel} is given by[17]:

$$C_{rel}=\frac{\mathrm{Re}(Y_j)}{\mathrm{Re}(Y_j+Y_p)}\,\frac{\mathrm{Re}(Z_{eq2})}{\mathrm{Re}(Z_{eq2}+Z_q)}\,\frac{\mathrm{Re}(Z_{eq1}^{-1})}{\mathrm{Re}(Z_{eq1}^{-1}+Y_p)}, \tag{9}$$

where $Y_p=Z_p^{-1}$, $Z_{eq2}=(Y_p+Y_j)^{-1}$ and $Z_{eq1}=Z_q+Z_{jeq2}$. The impedances Z_p and Z_q are given by

$$\begin{aligned} Z_q&=Z_0\sinh(\gamma l),\\ Z_p&=Z_0\coth(\gamma l). \end{aligned} \tag{10}$$

III. SURFACE IMPEDANCE

As was shown in the previous section, the surface impedance of the strip and the ground plane of the microstrip play an important role in the characterization of the microstrip. The surface impedance $Z_s(\omega)$ is defined by

$$Z_s(\omega)=\frac{E_x(0,\omega)}{\int_0^\infty J_x(z,\omega)dz}=R_s+jX_s, \tag{11}$$

where $E_x(0,\omega)$ is the electric field parallel at the surface of the conductor and $J_x(z,\omega)$ is the current density in the conductor at depth z. The characteristic length scales of field penetration into the metal are the resistive and reactive skin depths δ_r and δ_i, defined by the relations:

$$\delta_r=\frac{R_s}{\mu_0\omega},\quad \delta_i=\frac{X_s}{\mu_0\omega}. \tag{12}$$

The general behavior of Z_s depends on the value of $\omega\tau$ and the ratios l_e/δ_c in case of normal conductors and ξ/λ in case of superconductors.[18] Here l_e is the mean free path of the electrons, τ is the scattering time, δ_c is the classical skin depth $\sqrt{2/\omega\mu_0\sigma}$ ($=\delta_r/2$), ξ is the Pippard coherence length, and λ is the effective penetration depth ($=\delta_i$). The Pippard coherence length and the effective penetration depth are related to the coherence length ξ_0 and the London penetration depth λ_L via $\xi^{-1}=\xi_0^{-1}+l_e^{-1}$ and $\lambda=\lambda_L(\xi_0/\xi)^{1/2}$.[19] In the local limit where $l_e\ll\delta_c$ and $\xi\ll\lambda$, the current density J and the electric field E are related by the conductivity σ via $J=\sigma E$. The surface impedance Z_s of a material with thickness t, is then solved directly from Maxwell's equations and is given by

$$Z_s(\omega)=\sqrt{\frac{i\omega\mu_0}{\sigma}}\coth(\sqrt{i\omega\mu_0\sigma}t). \tag{13}$$

In the nonlocal case where $l_e\gg\delta_c$ and $\xi\gg\lambda$, the electric field inside the (super)conductor changes over the mean free path l_e or the superconducting coherence length ξ and more elaborate calculations are necessary. Mattis and Bardeen[16] derived the following relationship between the current density $\mathbf{J}$ and the vector potential $\mathbf{A}$ at the surface of a superconducting material

$$\mathbf{J}(r)=\frac{3}{4\pi^2 v_0\hbar\lambda_L^2}\int\frac{\mathbf{RRA}(\mathbf{r}')I(\omega,R,T)e^{-R/l_e}}{R^4}dV', \tag{14}$$

where $\mathbf{R}=\mathbf{r}-\mathbf{r}'$ is the vector from the point for which the current density is to be calculated to the volume element dV' and v_0 is the Fermi velocity. The kernel $I(\omega,R,T)$ is a complicated function which describes the energy and k-vector dependence of the scattering and creation of quasiparticle excitations at a temperature T. Expressions for $I(\omega,R,T)$ can be found in the original paper of Mattis and Bardeen. It can be shown that Eq. (14) reduces to Ohm's law when the field is constant over the mean free path, and the appropriate value of $I(\omega,R,T)$ in the normal state is used. In the nonlocal case the calculation of the surface impedance cannot be solved directly from the Maxwell's equations, because the (specular or diffuse) scattering of electrons at the surface has to be taken into account. This problem was solved by Reuter and Sondheimer.[20]

A thorough numerical calculation of the surface resistance Z_s, involving the complete Mattis–Bardeen equations of the anomalous skin effect and the Reuter–Sondheimer equations, is performed by Pöpel.[21] Instead of this complete (and very complex) solution, we use the extreme anomalous

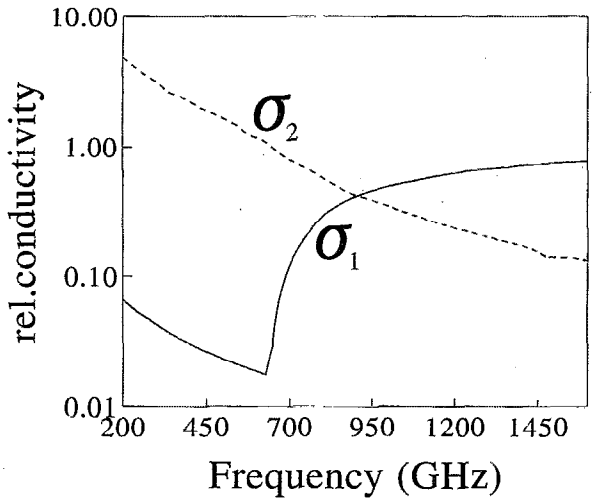

FIG. 2. Conductivities σ_1 and σ_2 as a function of frequency at $T=4.2$ K, for the niobium layers used in this work. The sharp increase in σ_1 is at the gap frequency.

limit ($\xi \gg \lambda$) of the Mattis–Bardeen theory, and two limiting cases of the Reuter–Sondheimer calculation. In the extreme anomalous limit a complex conductivity $\sigma_s=\sigma_1-j\sigma_2$ for the superconducting state is used [σ_s is the $R=0$ solution of $I(\omega,R,T)$]. The expressions for σ_1 and σ_2 (scaled to the normal state conductance σ_n) are:

$$\frac{\sigma_1}{\sigma_n}=\frac{2}{\hbar\omega}\int_{\Delta}^{\infty} dE[f(E)-f(E+\hbar\omega)] \times\frac{E^2+\Delta^2+\hbar\omega E}{\sqrt{E^2-\Delta^2}\sqrt{(E+\hbar\omega)^2-\Delta^2}}+\frac{1}{\hbar\omega}\int_{\Delta}^{\hbar\omega-\Delta} dE \times[1-2f(\hbar\omega-E)]\frac{\hbar\omega E-E^2-\Delta^2}{\sqrt{E^2-\Delta^2}\sqrt{(\hbar\omega-E)^2-\Delta^2}}, \quad (15)$$

$$\frac{\sigma_2}{\sigma_n}=\frac{1}{\hbar\omega}\int_{\Delta-\hbar\omega,-\Delta}^{\Delta} dE[1-2f(E+\hbar\omega)] \times\frac{E^2+\Delta^2+\hbar\omega E}{\sqrt{E^2-\Delta^2}\sqrt{(E+\hbar\omega)^2-\Delta^2}}. \quad (16)$$

We assume that the high frequency signals do not bring the superconductor in a nonequilibrium state and that therefore $f(E)$ is the equilibrium FermiDirac distribution at the ambient temperature T. The first term of Eq. (15) describes the scattering of thermally excited quasi-particles. The second term describes the scattering of quasi-particles created by Cooper-pair breaking and therefore is zero unless $\hbar\omega>2\Delta$, in which case the lower limit of the integral in Eq. (16) is $-\Delta$, instead of $\Delta-\hbar\omega$. Equation (16) describes the "kinetic inductance" of the surface, caused by the response of the Cooper pairs. Results of a numerical calculation of σ_1 and σ_2 at 4.2 K are shown in Fig. 2.

The Reuter–Sondheimer equation for the surface impedance in the extreme anomalous limit is

TABLE I. Material parameters of Nb, Cu, and NbN (all lengths are in nm).

	$\sigma(\Omega^{-1}\,\mathrm{m}^{-1})$	l_e	$l_e/\sigma(\Omega\,\mathrm{m}^2)$	λ_L	ξ_0	λ	ξ
Nb	1.25×10^7	5	3.7×10^{-16}	38	38	100	5
Cu	3×10^{10}	1.9×10^4	6×10^{-16}	...	...	...	...
NbN	7×10^5	0.38	6×10^{-16}	40	40	370	0.4

$$Z_s=\frac{1}{3^{1/2}\pi^{1/3}}(1+\sqrt{3}i)\left(\frac{9\omega^2\mu_0^2 l_e}{16\sigma}\right)^{1/3}. \quad (17)$$

In the local limit, the Reuter–Sondheimer solution is equal to Eq. (13). At very high frequencies relaxation time effects become important ($\omega\tau\geqslant1$) and a modification of Eqs. (13) and (17) is necessary. This is most likely to occur in the extreme anomalous limit and in this case the surface resistance becomes independent of σ and l_e and depends only on the Fermi-velocity v_F as $R_s=\frac{3}{4}\pi v_F 10^{-7}\approx0.3\ \Omega$.[18]

IV. COMPARISON OF SURFACE RESISTANCES OF Nb, NbN AND Cu.

An overview of the material and electromagnetic parameters at 800 GHz of three metals of interest is shown in Tables I and II. Cu is taken as an example of a good conducting metal and other metals as Au or Ag will have parameters of the same order of magnitude. NbN is chosen because of its high transition temperature of ≈15 K and therefore the high gap frequency of $\approx$ 1.2 THz. The data of Cu and NbN are from Refs. 7, 22, and 23 and the data of Nb are deduced from resistivity measurements of Nb strips just above the transition temperature. As can be seen from Table II, relaxation time effects are unimportant for Nb and NbN, but could play a role in Cu. Furthermore, Nb and NbN are in the local limit ($l_e/\delta_c\ll1$), whereas Cu is in the extreme anomalous limit. Since we are interested in frequencies above 750 GHz and a temperature of 4.2 K, the classical skin depth in good conducting normal metals (as gold or copper with $\sigma\approx10^9$, $10^{10}\ \Omega^{-1}\,\mathrm{m}^{-1}$) will always be of the order of several tens of nm. This is much smaller than the mean free path, which is of the order of several μm and therefore the extreme anomalous limit of the Reuter–Sondheimer solution has to be used. It is important to notice that in this limit the frequency dependence of Z_s goes as $\omega^{2/3}$ instead of $\omega^{1/2}$ in the local limit and that Z_s depends on the ratio l_e/σ (which is a material constant *independent* of temperature) rather than on σ. It can be shown with a simple free electron model that l_e/σ is dependent on the electron density n via $n^{-2/3}$ and therefore will not vary much between different metals.[18] For example,

TABLE II. Electromagnetic parameters (order of magnitude) of normal conducting Nb, Cu, and NbN at 750 GHz.

	$\omega\tau$	δ_c(nm)	l_e/δ_c	ξ/λ
Nb	~0.05	~150	~0.03	0.05
Cu	~100	~10	~2000	...
NbN	~0.005	~800	~0.005	0.001

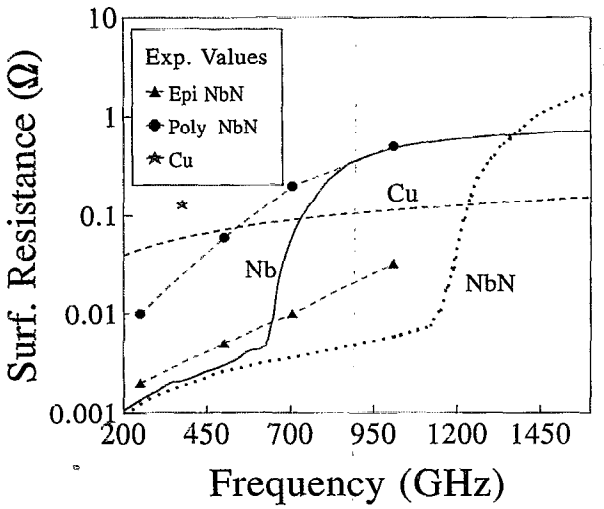

FIG. 3. Calculated surface resistance for Nb, NbN, and Cu at 4.2 K and measured data on Cu and (polycrystalline and epitaxial) NbCN films. The data on the NbCN and Cu are from Refs. 24 and 25.

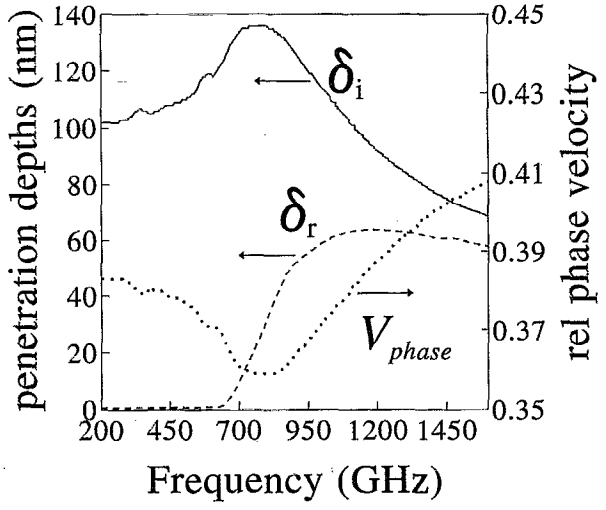

FIG. 4. Resistive δ_r and reactive δ_i penetration depths of Nb at 4.2 K. For ideal superconductors, the value δ_i for $F \to 0$ equals the London penetration depth. Also shown is the relative (to c, the speed of light) phase velocity. Notice the dispersion above 300 GHz.

the value of $l_e/\sigma = 3.7\times10^{-16}\ \Omega\ \mathrm{m}^2$ for Nb differs by only a factor of 2 from the l_e/σ value of copper ($=6\times10^{-16}\ \Omega\ \mathrm{m}^2$).

Results of calculations of the surface resistance R_s of Cu, Nb, and NbN at the frequency range of interest are shown in Fig. 3, together with some experimental data on NbN and Cu films. The sharp increase of the calculated surface resistance near the gap frequencies of the superconductors is clearly visible. Below their gap frequencies, Nb and NbN have the lowest loss and the surface resistance is only 5% of R_s(Cu). Above 1.2 THz Cu has the lowest R_s, which is about 15% of R_s Nb. In the frequency range of 700–1200 GHz the surface resistance of Cu is approximately 4 times lower than R_s(Nb). It can be seen that although the dc conductivities of Nb, NbN, and Cu differ orders of magnitude at 4.2 K, their rf surface resistances differ only slightly. The figure also shows some recent measurements on the surface resistance of Cu and (epitaxial and polycrystalline) NbCN films.[24,25] As can be seen, the experimental data of the Cu and the epitaxial NbCN film are in reasonable agreement with the theory, but the polycrystalline NbCN film has surface resistances which are orders of magnitude larger than calculated. The total absorption of power due to these surface resistances and the influence on the noise temperature of a practical SIS receiver will be discussed in the next section.

The frequency dependence of the characteristic penetration depths δ_r and δ_i for Nb are shown in Fig. 4. The resistive skin-depth is zero below the gap, then makes a steep increase in the 600–1000 GHz range and subsequently approaches the value of δ_r for normal conducting Nb at very high frequencies. The reactive skin depth (λ) is constant at low frequencies (100 nm) but gradually increases in the 400–800 GHz range, showing a maximum of 140 nm at 800 GHz. After this maximum the reactive skin-depth also approaches the δ_i value of normal conducting Nb at very high frequencies. The frequency dependence of the phase velocity for a typical stripline used in this work, is shown as the dotted line in Fig. 4. Since the phase velocity is proportional to $Z^{-1/2}$, it will be constant below 300 GHz and the stripline will be dispersion-free. Above 300 GHz the phase velocity becomes frequency dependent, and dispersion occurs.

A. Stripline loss and receiver noise temperature

With use of the theoretical surface resistances of Nb, NbN, and Cu, we now calculate a minimum achievable double side band (DSB) noise temperature of a practical SIS receiver with an integrated tuning structure. Based on state of the art SIS receivers at frequencies near the gap frequency [2–4,26] we make the assumption that the used Nb junctions have an area of 1 $\mu\mathrm{m}^2$ and that integrated tuning is necessary to achieve an efficient coupling of the high frequency signals. The total receiver noise temperature, expressed in noise and loss terms of the rf, mixer, and intermediate frequency (IF) components is given by

$$T_{\mathrm{REC}} = T_{\mathrm{RF}} + \frac{T_{\mathrm{MIX}}}{L_{\mathrm{RF}}} + \frac{T_{\mathrm{IF}}}{L_{\mathrm{RF}}\, L_{\mathrm{MIX}}}. \tag{18}$$

The main influence of the loss in the stripline is a decrease of the rf-input loss term L_{RF}. The noise contribution of the rf-input, T_{RF}, is hardly influenced, because the loss is at an ambient temperature of 4.2 K. The rf input noise and the IF amplifier noise are independent of frequency and will have typical values of $T_{\mathrm{RF}}=40$ K and $T_{\mathrm{IF}}=4$ K, respectively. The frequency dependence of the mixer conversion loss and noise is approximated by $L_{\mathrm{MIX}}(f)=100/f$ and $T_{\mathrm{MIX}}(f)=0.075f$ ($\approx$ 3/2 times Quantum Limit),[27] with f in GHz and f smaller than $2f_{\mathrm{gap}}$ of Nb ($\approx$ 1400 GHz). We divide the loss of the rf-input circuit into a frequency independent loss $L_{\mathrm{RF}}^{\mathrm{opt}}$, formed by the optical input (dewar-window, heatfilter, antenna, waveguide) and a frequency dependent loss $L_{\mathrm{RF}}^{\mathrm{line}}(f)$, given by the frequency dependent loss in the stripline. A typical value for the optical rf loss is $L_{\mathrm{RF}}^{\mathrm{opt}}=0.75$. The exact value of $L_{\mathrm{RF}}^{\mathrm{line}}(f)$ depends not only on the material parameters but also on the design of the inte-

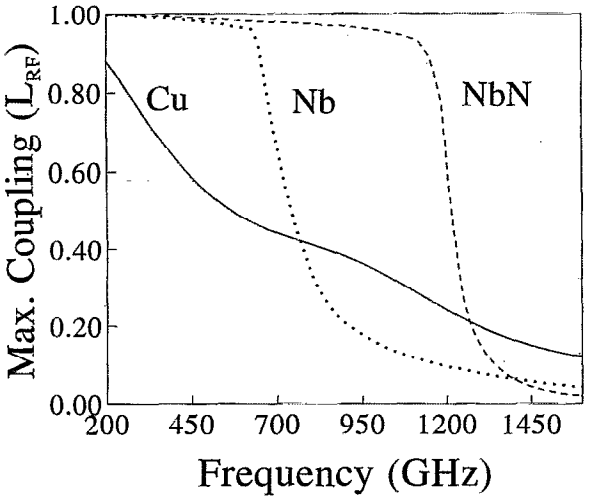

FIG. 5. Calculated maximum coupling of striplines made of Nb, NbN, and Cu as a function of frequency.

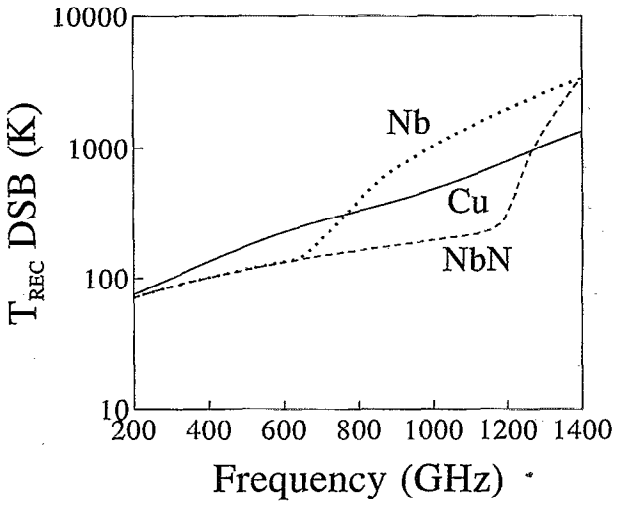

FIG. 6. Calculated minimum receiver noise temperature of a heterodyne receiver as a function of frequency. The noise temperature is based on the maximum coupling shown in Fig. 5.

grated tuning structure; a wide stripline will have lower current densities than a narrow line and therefore has lower loss, and the loss is proportional to the length. The tuning structure we use in the calculation of L_{RF}^{line} has a fixed length (designed for 800 GHz) and is of the end-loaded type (this tuning structure will be discussed in the next section). Other types of tuning structures have a somewhat different loss behavior, but the general frequency dependence will be the same. Since the phase velocities in Nb, NbN, and Cu striplines differ due to the differences in material parameters, the striplines have different lengths for the 800 GHz design frequency and the calculated length of the striplines is 40, 24, and 54 μm for Nb, NbN, and Cu, respectively. Calculations show that in the frequency range of interest the total loss in the stripline depends only weakly on the stripline length. The error in L_{RF}^{line} introduced by keeping the length of the line fixed, instead of varying it with the desired resonance frequency, is therefore minimal.

Results of the calculated frequency dependence of the loss L_{RF}^{line} at 4.2 K, obtained with Eqs. (13), (15), (16), (17), and for a junction with a resistance of 16 Ω, are shown in Fig. 5. As was already shown in Fig. 3 the surface resistance of the Nb and NbN layers below the gap frequency is very low, and $L_{RF}^{line} \approx 1$. Above the gap L_{RF}^{line} decreases rapidly as a function of frequency, to a value of less than 0.05 at 1.4 THz. The Cu stripline shows a monotonic decrease of L_{RF}^{line} as a function of frequency. At $\approx$800 GHz, the frequency above which the Cu stripline starts to outperform the Nb stripline, L_{RF}^{line} of this line is 0.4.

The results of the calculated receiver noise temperature, using Eq. (18) and the values for the various noise and loss contributions given above, is shown in Fig. 6. The figure shows that receivers with Nb and NbN striplines can achieve a minimum noise temperature of approximately three times the quantum limit below the gap frequency of the stripline material. Above the gap frequency the minimum achievable noise temperature increases rapidly and in this region the *noise* temperature is nearly proportional to $(L_{RF}^{line})^{-1}$, showing the importance of a low loss matching circuit. The minimum noise temperature achievable with normal metal striplines goes from 300 to 1000 K in the 800–1200 GHz range. The data shown in Fig. 6 are based on idealized material parameters and surface resistances, and it is important to notice that these calculations neglect, for example, the influence of surface irregularities or the differences between polycrystalline and epitaxial NbN films. As is shown in Fig. 3 the surface resistance of a measured polycrystalline NbCN film is much higher than predicted and at frequencies of interest even worse than Cu. If these values are typical for polycrystalline Nb(C)N films, then only epitaxial grown Nb(C)N films can be used at THz frequencies.

V. EXPERIMENTAL DETAILS

The frequency dependent radiation coupling of the resonator formed by the junction and the tuning structure is measured with a Fourier transform spectrometer. The SIS junction is used as a direct detector (with a current responsivity $R = \Delta I/\Delta P = e/\hbar\omega$[28]), which probes the coupling to the resonator. The junction is voltage biased at a voltage just below the gap voltage. The measured interferogram is the modulation of the junction current caused by the chopped blackbody input power, as a function of the position of one of the mirrors of the interferometer. The Fourier transform of this interferogram gives the frequency response of the receiving system. This includes the efficiency of the following components: the optical system (window, heatfilter, lens), the waveguide system (RF filter, backshort tuner), the current responsivity of the junction and the coupling of the tuning structure.

The FTS measurements are performed with a Michelson interferometer with a Hg-arc lamp as source (chopped with a frequency of 16 Hz) and a 50 μm Kapton beam-divider. The double sided interferograms are measured with an optical stepsize of 80 μm and a total mirror movement of 2 cm. This yields a resolution of approximately 7 GHz. The typical in-

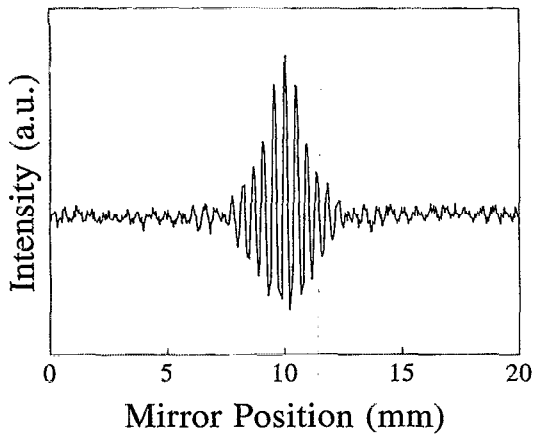

FIG. 7. Interferogram measured with Michelson interferometer on the sample with the two-section stub.

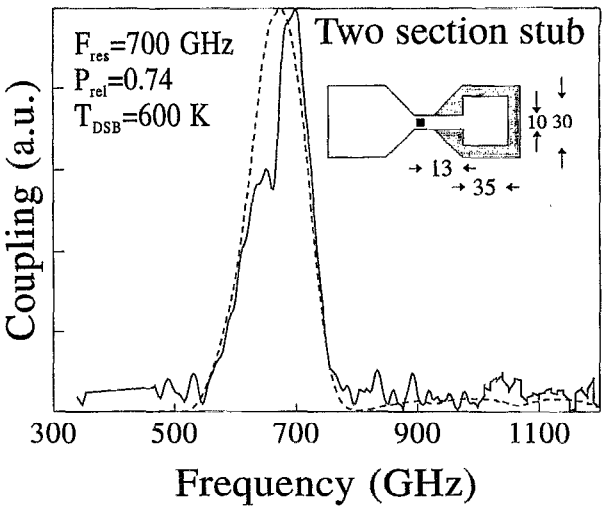

FIG. 8. Measured (solid line) and calculated (dashed line) frequency response of the two-section integrated tuning structure. Measurements and calculations are scaled to another. The inset shows the geometry of the tuning structure. Dimensions are in μm.

tegration time is 1 s. The total incident power level on the device is that low (~nW) that we do not expect any heating effects.

The Nb tunnel junctions (with an area of 1 ± 0.1 μm^2, a specific capacitance of 55 ± 5 fF/μm^2 and a normal resistance of 16 Ω) are fabricated with the use of a process described elsewhere.[29] The gap voltage of the junctions was only 2.5 meV at 4.2 K, which corresponds to a gap frequency of 603 GHz. We assume that the Nb layers forming the stripline have the same gap as measured with the tunnel junction. Material parameters at 4.2 K of typical Nb layers are shown in Table I. The thicknesses of the Nb layers forming the ground plane and the microstrip of the tuning structures is 200 and 600 nm, respectively. The SiO_2 dielectric between these layers is 250 nm thick and has a relative dielectric constant ϵ_r of 3.8. The main width of the striplines used in this work is 10 μm, yielding a characteristic impedance of $Z_0=7$ Ω. The junctions and the tuning structures are fabricated, together with a band-stop rf filter, on a 200-μm-thick fused quartz substrate. After fabrication the quartz is polished down to 45 μm and diced in widths of 90 μm. The substrates are glued in the substrate channel of the mixerblock, perpendicular to the sidewall of the waveguide. The mixerblock consists of a full height waveguide with dimensions 300×150 μm and a substrate channel of dimensions 100×100 μm (perpendicular to the waveguide). One end of the waveguide is closed by an adjustable backshort tuner and the other end contains a transition to a diagonal horn. Some details of the mixerblock are shown in Fig. 1(b). The mixerblock is placed on the cold plate of a liquid He dewar and the signals enter the dewar via a 1-mm-thick TPX window and a 190 μm quartz heat-filter. The radiation coupling to the horn is provided by a polyethylene lens. This measurement set-up is the same as the one we use to perform heterodyne mixing measurements.[2,30]

VI. RESULTS

The measured interferogram of one of the matching circuits (two-section stub) is shown in Fig. 7 and the measured coupling of the three tuning structures is shown in Figs. 8, 9, and 10, together with the calculated frequency responses, which will be discussed later.

The signal to noise ratio is good and the Fourier transforms clearly show the peaks in coupling near the calculated resonance frequencies. The coupling of the end-loaded stub is so broadband that in this measurement the cut-off frequency of the waveguide at 460 GHz is observed. The observed decrease in coupling near 560 GHz in this measurement and the dip in the coupling near 670 GHz in Fig. 8 are due to strong absorption lines of H_2O vapor, present in the laboratory.[31] The other modulations of the coupling below 700 GHz are probably due to the frequency dependence of

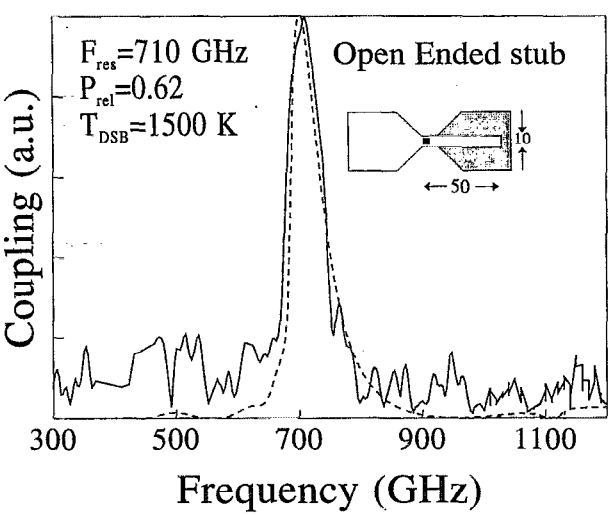

FIG. 9. Measured (solid line) and calculated (dashed line) frequency response of the open-ended integrated tuning structure. Measurements and calculations are scaled to another. The inset shows the geometry of the tuning structure. Dimensions are in μm.

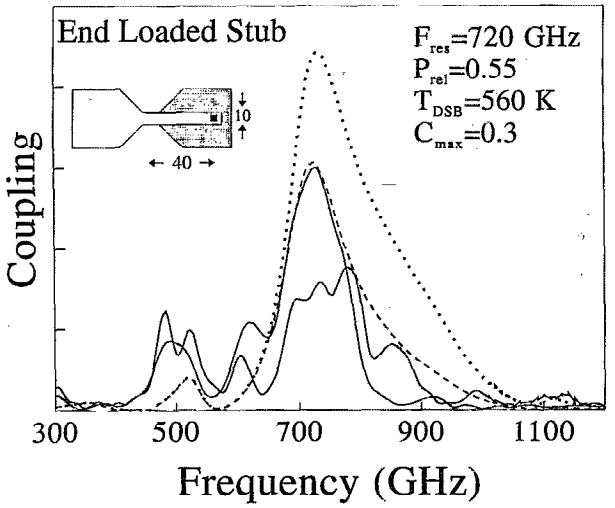

FIG. 10. Measured (solid lines) and calculated absolute frequency response of the end-loaded integrated tuning structure. The dotted line is the response calculated using the original Mattis–Bardeen solution. The dashed line is the Mattis–Bardeen solution with a steeper absorption edge above the gap. Measurements are shown for two different backshort positions.

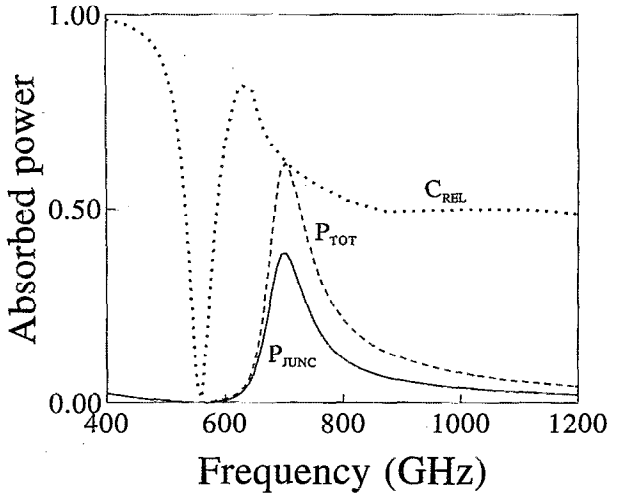

FIG. 11. Calculated frequency response of open-ended tuning stubs, using a model in which the source impedance (of the waveguide mount) is kept constant at 50 Ω. P_{tot} is the power coupled to the resonator, P_{junc} is the actual power coupled to the junction. At the dip at 560 GHz, the line is $\lambda_g/4$ long, effectively shorting the junction at the rf frequency.

the rf filter. The rf filter of this junction has a center frequency of 850 GHz and below 700 GHz the impedance of the filter (and thus the leakage into the substrate channel) varies strongly as a function of frequency.

The differences in bandwidth of the three tuning structures are clearly observed. The bandwidth of the open-ended stub is 75 GHz and the end-loaded and two-section stub have bandwidths of 125 and 200 GHz, respectively. In the displayed measurements the backshort setting has been optimized for maximum coupling of the signal. Measurements at different settings of the backshort showed that the frequency dependence and the bandwidth of the coupling are mainly determined by the stubs and not by the backshort tuner. Figure 10 includes the coupling of the end-loaded stub at one backshort position other than the optimum setting. The main influence is a decrease in maximum coupling and a slight increase in the coupling at higher frequencies. No coupling at frequencies above 940 GHz is observed.

The three structures were also tested as heterodyne mixing elements. The two-section and the end-loaded stub have comparable minimum DSB noise temperatures of 600 K (@ 700 GHz) and 560 K (@720 GHz), respectively, measured at a bath temperature of 4.2 K. The noise temperature of the end-loaded stub dropped to 400 K when the bath temperature was lowered to 2 K. The performance of the mixer with the end-loaded stub is also measured at 840 GHz and shows a noise temperature of 1500 K at that frequency. The performance of the open-ended stub is not as good, and has the lowest noise temperature of 1500 K DSB at 700 GHz.[2] An analysis of the heterodyne measurements with the end-loaded stub, shows that the loss due to this tuning structure is approximately 70%. Based on the comparable noise temperatures we expect that the loss of the two-section stub will be of the same order.

VII. DATA ANALYSIS

In the analysis of the measured results we first use a simple model in which the resonator is coupled to a frequency independent source with an output impedance of 50 Ω (the tuning capability and frequency dependence of the waveguide system are thus ignored). The loss in the striplines is calculated by using the method described in Sec. II. The results of this calculation for the open-ended and the end-loaded stub are shown in Figs. 11 and 12. The two-section stub has the same qualitative behavior as the open-ended stub.

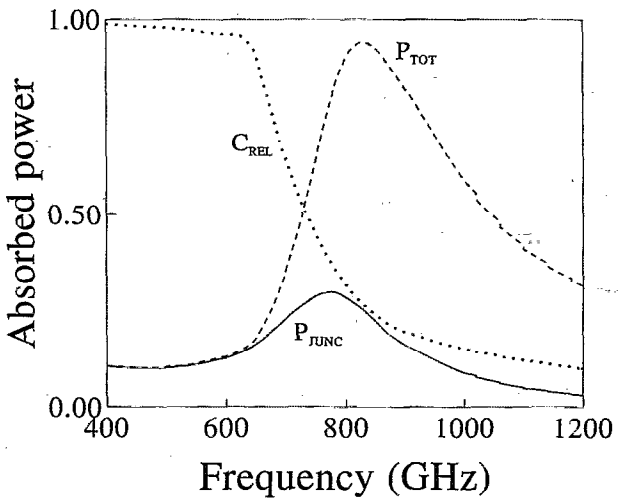

FIG. 12. Same as in Fig. 11, but now for end-loaded tuning structure. Note the difference between the frequency with maximum coupling to the whole resonator, and the frequency at which the coupling to the junction is at optimum.

The figures display three curves: the dashed curve indicates the amount of coupled power into the junction and the stripline (P_{tot}), where the available power of the signal source is normalized to 1, the dotted curve gives the relative amount of this power coupled into the junction (C_{rel}), and the solid curve ($=P_{tot}\times C_{rel}$) is the actual amount of power coupled into the junction (P_{junc}). The resonance frequency of the open-ended stub is 706 GHz, with $C_{rel}=0.62$ and a bandwidth of 80 GHz. For the two-section stub (not displayed) we find : $F_{res}=706$ GHz, $C_{rel}=0.74$ and $\Delta F=120$ GHz. These numbers agree very well with the measured FTS data and with the observation that the frequency response of these stubs is not influenced by the backshort setting.

Under the assumption that the waveguide tuner is capable of achieving a nearly perfect match to the resonator system, one would expect that the open-ended and the two-section stub resonators will have nearly equal performance in a heterodyne measurement. This is not observed and we attribute this to the limited tuning range of the backshort tuner and the differences in the rf filters of the used samples.

As can be seen in Figs. 11 and 12 the striplines are nearly lossless below the gap frequency ($P_{junc}=P_{tot}$) and the amount of power dissipated in the junction equals the amount of coupled power (the low coupling of the open-ended stub below the resonance is caused by the initial capacitive behavior of this type of stub at low frequencies). This situation changes above the gap frequency, where both the stripline and the junction dissipate part of the coupled power. The effect of this dissipation in the case of the open-ended stripline is an overall decrease in coupling, but there is no noticeable shift of the resonance frequency of the power coupling in the junction. Calculations on the end-loaded stub show that in this case a large difference exists between the resonance frequency of the total resonator system (830 GHz) and the frequency at which the optimum power coupling into the junction occurs (770 GHz). The relative power coupling at 770 GHz is 0.35 with a bandwidth of 255 GHz. Contrary to the open-ended stub, this frequency is directly influenced by the absorption edge of the superconducting stripline above the gap frequency. A steeper absorption edge not only reduces the maximum coupling, but also reduces the frequency at which this maximum coupling is observed.

In the final analysis of the measured data the frequency dependence of the waveguide and the rf filter are taken into account by using a model for the waveguide mount, described in Refs. 32 and 33. In this model the electromagnetic environment of the junction is represented by an equivalent circuit, shown in Fig. 1(c). The frequency dependent impedance of the waveguide $Z_g(f)$ and the backshort tuner $Z_{bs}(f)$ in this model are given by

$$Z_g(f)=\frac{377}{\sqrt{1-f_c^2/f^2}}\ \Omega, \tag{19}$$

$$Z_{bs}(f)=jZ_g(f)\tan\left(\frac{2\pi f l_b}{c}\sqrt{1-f_c^2/f^2}\right)\Omega, \tag{20}$$

where f_c is the waveguide cut-off frequency (460 GHz in this work), c is the speed of light, and l_b is the position of the backshort (in m).[34]

The π-network of Z_1, Z_2, and Z_3+Z_{RF} gives the equivalent circuit for the combination of the waveguide probe, the substrate channel, and the rf filter. The frequency dependence of Z_{RF} is calculated with an equivalent microstrip model of the rf filter, based on equations given in Ref. 17. The model described above gives only a qualitative description of the real frequency dependence of the waveguide mount, because the exact values for Z_1, Z_2, and Z_3+Z_{RF} are unknown and also vary as an unknown function of frequency. The values we use ($Z_1=Z_3=-j100\ \Omega$, $Z_2=j100\ \Omega$) are based on values obtained with scale model measurements on a comparable waveguide mount.[32]

The results for the calculated response, using the model which includes the (approximated) frequency response of the waveguide mount, are shown in Figs. 8, 9, and 10. Figure 10 displays the results of the calculated coupling of the end-loaded stub, using the stripline parameters obtained by the extreme anomalous limit of the Mattis–Bardeen theory and the assumption that the tuner can achieve a nearly perfect match to the resonator (the coupling into the junction P_{junc} then equals C_{rel}). The maximum coupling calculated with the original stripline parameters (0.55 at 720 GHz) is about a factor of 2 higher than the value obtained from the heterodyne measurements (0.3), and the calculated curve predicts coupling at frequencies much higher than observed. At 840 GHz, the original design frequency, the measured coupling is only 6%. As shown previously, this can be explained by the underestimation of the steepness of the fall-off of the absorption of the stripline above the gap frequency. We find that if we raise C_{rel} to the power 1.6, a much better agreement between the measured and calculated curves is found, both on the absolute coupling and on the fall off at higher frequencies. This is the dashed line in Fig. 10. The calculated results of the end-loaded stub below 700 GHz are strongly influenced by the assumptions on the rf-filter impedance, but the general agreement, especially the onset of the coupling at 460 GHz, is reasonable. The results for the two-section and open-ended stub, have to be scaled to the measured results, because we have no absolute calibration of our FTS measurement setup, nor do we have a precise knowledge about the impedance parameters describing the waveguide mount. With the same adjustment on the absorption, a good qualitative agreement between calculation and measurement is also found for these stub types.

The observation of a steeper absorption edge than calculated with the extreme anomalous limit of the Mattis–Bardeen theory was also observed by previous workers on Nb films.[14,35] As pointed out by Pöpel,[21] this discrepancy is caused by using the extreme anomalous limit outside the parameter range where this theory is valid. This is also the case in our experiments, where the requirement that the Pippard coherence length should be much larger than the penetration depth is certainly not fulfilled. For a more detailed description of Nb striplines above the gap frequency, the full Mattis–Bardeen theory should therefore be used.

The theoretical predictions on the receiver noise temperatures of a mixer with a Nb tuning structure, shown in Fig. 6, underestimate the measured noise temperatures at 720 and 840 GHz considerably. Since this is mainly caused by

the steep decrease of L_{RF}^{line} above the gap frequency it is of major importance to investigate the loss behavior of normal metal or NbN striplines in the THz frequency regime.

VIII. CONCLUSION

In conclusion, we have demonstrated that Nb resonator systems can be used at frequencies above the gap frequency and that the bandwidth and resonance frequency are well described by the extreme anomalous limit of the Mattis–Bardeen theory. Our measurements indicate that the increase in loss above the gap frequency is significantly higher than calculated. For frequencies above 800 GHz the maximum coupling with our Nb films is lower than 10%. This loss has a major drawback on the performance of SIS heterodyne receivers and above 800 GHz the use of normal metal or (epitaxial) NbN as basis material for the striplines should be investigated. We have shown that with the use of low loss tuning structures the use of SIS mixers can be extended to the THz frequency regime and that receiver noise temperatures below 600 K at 1 THz seem to be achievable.

ACKNOWLEDGMENTS

We gratefully acknowledge the excellent work done by C. E. Honingh and H. H. A. Schaeffer in developing the microwave setup used in these experiments. We thank M. Dierichs, J. Feenstra, and J. Wijnbergen for the initial help with the Michelson measurements. We also thank Van Duc Nguyen and H. Golstein for technical support in the preparation of these experiments. This work is financially supported by the European Space Agency under contract No. 7898/88/NL/PB(SC) and the Stichting voor Technische Wetenschappen and the Stichting voor Fundamenteel Onderzoek der Materie.

[1] A. V. Räisänen, W. R. McGrath, P. L. Richards, and F. L. Lloyd, IEEE Trans. Microwave Theory Techn. **MTT-33**, 1495 (1985).
[2] G. de Lange, C. E. Honingh, J. J. Kuipers, H. H. A. Schaeffer, R. A. Panhuyzen, T. M. Klapwijk, H. van de Stadt, and M. W. M. de Graauw, Appl. Phys. Lett. **64**, 3039 (1994).
[3] J. Zmuidzinas, H. G. LeDuc, J. A. Stern, and S. R. Cypher, IEEE Trans. MTT **42**, 698 (1994).
[4] H. Rothermel, K. H. Gundlach, and M. Voss, J. de Physique **4**, 267 (1994).
[5] S. Sridhar, J. Appl. Phys. **63**, 159 (1988).
[6] J. Halbritter, Z. Physik **266**, 209 (1974).
[7] R. L. Kautz, J. Appl. Phys. **49**, 308 (1978).
[8] R. L. Kautz, J. Research NBS **84**, 247 (1979).
[9] H. H. S. Javadi, W. R. McGrath, and H. G. LeDuc, J. Appl. Phys. **61**, 2712 (1992).
[10] Qing Hu, C. A. Mears, and P. L. Richards, Phys. Rev. B **42**, 10250 (1990).
[11] M. M. T. M. Dierichs, B. J. Feenstra, A. Skalareand C. E. Honingh, J. Mees, H. van de Stadt, and Th. de Graauw, Appl. Phys. Lett. **63**, 249 (1993).
[12] R. E. Glover III and M. Tinkham, Phys. Rev. **104**, 844 (1956).
[13] P. L. Richards and M. Tinkham, Phys. Rev. Lett. **1**, 318 (1958).
[14] S. L. Norman, Phys. Rev. **167**, 393 (1968).
[15] M. C. Nuss, K. W. Goossen, J. P. Gordon, P. M. Mankiewich, and M. L. O'Malley, J. Appl. Phys. **70**, 2238 (1991).
[16] D. C. Mattis and J. Bardeen, Phys. Rev. **111**, 412 (1958).
[17] T. C. Edwards, *Foundations for Microstrip Circuit Design* (Wiley, Chisester, 1981).
[18] A. B. Pippard, in *Advances in Electronics and Electron Physics*, edited by L. Marton (Academic, New York, 1954), p. 1.
[19] M. Tinkham, *Introduction to Superconductivity* (McGraw-Hill, New York, 1975).
[20] G. E. H. Reuter and E. H. Sondheimer, Proc. R. Soc. Ser. A **195**, 336 (1984).
[21] R. Pöpel, J. Appl. Phys. **66**, 5950 (1989).
[22] C. C. Chin, D. E. Oates, G. Dresselhaus, and M. S. Dresselhaus, Phys. Rev. B **45**, 4788 (1992).
[23] D. E. Oates, A. C. Anderson, C. C. Chin, J. S. Derov, G. Dresselhaus, and M. S. Dresselhaus, Phys. Rev. B **43**, 7655 (1991).
[24] S. Kohjiro, S. Kiryu, and A. Shoji, IEEE Trans. Appl. Supercond. **3**, 1765 (1993).
[25] J. D. Cook, J. W. Zwart, K. J. Long, V. O. Heinen, and N. Stankiewicz, Rev. Sci. Instrum. **62**, 2480 (1991).
[26] W. R. McGrath, P. Febvre, P. Batelaan, H. G. LeDuc, B. Bumble, M. A. Frerking, and J. Hernichel, in *Proceedings of the Fourth International Symposium on Space THz Technology* (UCLA Press, Los Angeles, CA, 1993), p. 50.
[27] W. C. Danchi and E. C. Sutton, J. Appl. Phys. **60**, 3967 (1986).
[28] J. R. Tucker and M. F. Millea, Appl. Phys. Lett. **33**, 611 (1978).
[29] M. M. T. M. Dierichs, R. A. Panhuyzen, C. E. Honingh, M. J. de Boer, and T. M. Klapwijk, Appl. Phys. Lett. **62**, 774 (1993).
[30] G. De Lange, C. E. Honingh, M. M. T. M. Dierichs, H. H. A. Schaeffer, J. J. Kuipers, R. A. Panhuyzen, T. M. Klapwijk, H. van de Stadt, M. W. M. de Graauw, and E. Armandillo, *Proceedings of the Fourth International Symposium on Space THz Technology* (UCLA Press, Los Angeles, CA, 1993), Vol. 3, p. 41.
[31] T. G. Phillips and J. Keene, Proc. IEEE. **80**, 1662 (1992).
[32] C. E. Honingh, G. de Lange, M. M. T. M. Dierichs, H. H. A. Schaeffer, Th. de Graauw, and T. M. Klapwijk, IEEE Trans. MTT **41**, 616 (1993).
[33] A. V. Räisänen, Int. J. Infrared & MM Waves **6**, 1169 (1985).
[34] R. E. Collin, *Foundations for Microwave Engineering, Physical and Quantum Electronics Series* (McGraw-Hill, New York, 1966).
[35] P. L. Richards and M. Tinkham, Phys. Rev. **119**, 575 (1960).